



Flexible film-based thermoelectric generators

Shuping lin¹, Wei Zeng¹, Lisha Zhang¹, Xiaoming Tao^{1*}

Research Center of Smart Wearable Technology, Institute of Textile and Clothing, The Hong Kong Polytechnic University, Hong Kong SAR, China PR

*Corresponding author: xiao-ming.tao@polyu.edu.hk

ABSTRACT:

*The present work highlights the progress in the field of flexible thermoelectric generator (f-TEGs) fabricated by 3-D printing strategy on the typing paper substrate. In this study, printable thermoelectric paste was developed. The dimension of each planer thermoelectric element is 30mm*4mm with a thickness of 50 μm for P-type Bismuth Tellurium (Bi_2Te_3)-based/ poly(3,4-ethylenedioxythiophene) polystyrene sulfonate (PEDOT:PSS) leg. A single thermoleg with this dimension can generate a voltage of 5.38 mV at a temperature difference of 70 K. The calculated Seebeck Coefficient of a single thermoleg is 76.86 $\mu\text{V/K}$. This work demonstrates that low-cost printing technology is promising for the fabrication of f-TEGs.*

Introduction:

In recent years, a rapidly increasing research progress has been made in flexible TEGs because of its remarkable application potentials in energy harvesting, [1-4] micro-robotics, and electronic textiles.[5-7] However, the fabrication of inorganic thermoelectric materials into thermoelectric modules involves high-temperature, long-term and high-cost processes. Moreover, it is a grand challenge to integrate these rigid inorganic materials into flexible TEG which requires unusual topology for an enhanced practical efficiency.[8, 9]

Conducting polymers, such as Poly(3,4-ethylenedioxythiophene)-poly(styrenesulfonate) (PEDOT:PSS), have unique properties for TE application as their low thermal conductivity, solution processability for large-scale fabrication, low processing cost for manufacturing devices and application potential as flexible and lightweight devices. [10-12] Inorganic materials, such as Bismuth Telluride (Bi_2Te_3) is the best-known commercially used thermoelectric material for power generation applications owing to their high power factor at room temperature. [13, 14] Recently, flexible TE sheets and nonwoven fabrics based on poly-(styrenesulfonate)-doped poly(3,4-ethylenedioxythiophene), [15] doped carbon nanotube sheets, [16] and graphene composites [17-19] have been demonstrated in recent pioneering work. The Byung Jin Cho Group at the Korea Advanced Institute of Science and Technology has developed a glass fabric-based thermoelectric generator. But the TE elements in this structure are neither very flexible nor yarn based. [10] The progress of truly flexible composite-based flexible thermoelectric devices demonstrated that this principle could significantly enhance the device conversion of waste heat into electricity, applying the devices to any kind of objects with any kind of shapes. [20] Synergetic combination of the easy processability of PEDOT:PSS and the excellent thermoelectric performance of Bi_2Te_3 can obtain an increased electric conductivity and more uniform TE film. In stark contrast to rigid inorganic materials, this inorganic-polymer strategy is facile synthesis and solution processable which can fit the 3-D printing requirement for the TEGs. Taking advantage of the flexibility of the PEDOT:PSS and using these “molecular inks” to connect with rigid materials can produce flexible thermoelectric devices.

Experimental section:

Materials. P-type Bi_2Te_3 (99.99%, KYD Materials), poly(3,4-ethylenedioxythiophene) polystyrene sulfonate (PEDOT:PSS, 5.0 wt. %, Sigma Aldrich), dimethyl sulfoxide (DMSO, 99.9% %, VWR chemicals), ethanol (EtOH, 99.8%, VWR Chemicals), α -terpineol (96%, Alfa Aesar), isopropanol (AR, UNI-CHEM) were purchased commercially and used without further purification.

p-type Bi_2Te_3 / PEDOT:PSS paste preparation. The paste consists of 3.07 g metal powders (P-type Bi_2Te_3), 0.4g DMSO, 2.0g PEDOT:PSS, 0.43g isopropanol and 0.46g α -terpineol. The pastes were thoroughly mixed for 12h using magnetic stirrer. The solvent maintains the paste's viscosity at a desired level and used to mix the powders. DMSO solvent was added to the PEDOT:PSS solution to improve the electrical conductivity. Device fabrication and characterization. First, the Bi_2Te_3 film (p-type) legs were printed on a flexible Polyimide (PI) paper and typing paper. The thickness of the TE legs was 50 μm . After the printing step, the printed film was dried to remove organic residues. In order to evaluate the output characteristics of the fabricated TEG module, the exact temperature difference of both sides of the module must be known. In this work, a measuring apparatus using a heater at the hot side and a cooler at the cold side was used. The output voltage and temperature difference of the module was measured by a Keithley 2700 equipment and Anbat AT4516 simultaneously.

Results and discussion:

Thermoelectric film morphology

In this work, p-type Bi_2Te_3 / PEDOT:PSS paste was used to coat on PI fibers and print on PI paper, respectively. In previous study, p-type Bi_2Te_3 / PEDOT:PSS paste was coated on the PI fibers to see the adhesiveness between the materials and substrate. Figure 1 shown the PEDOT:PSS coated PI fiber and p-type Bi_2Te_3 / PEDOT:PSS coated PI fiber. The surface and the cross-section of the coated yarn and printed film were observed in a Scanning Electron Microscope (SEM, Tescan VEGA3). From the SEM images (Figure. 1a-d), a continuous uniform PEDOT:PSS coating on the surface of PI yarn was observed, which providing continues tunnels for electron transport. In this light, this PEDOT:PSS conducting polymer can be used to incorporate nano-scaled inorganic materials act as polymer matrix for TE properties. The SEM images of Figure. 1 (e-h) showed the homogenous mixture of p-type Bi_2Te_3 and PEDOT:PSS. Also, the average of particle size can be identified to be around 10 μm . The thickness of TE coating was approximately 200-300 μm . The twisted structure of PI yarn caused the inhomogeneous thickness of the TE coating. Thus, in contrast to rigid inorganic materials, this inorganic-polymer strategy facilitates facile synthesis and solution accessibility, which meets the printing requirements for the f-TEGs fabrication.

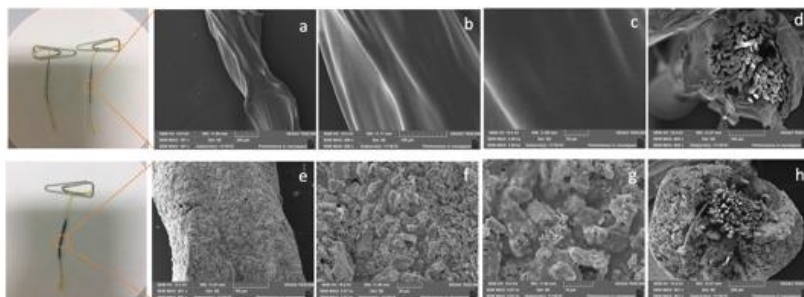


Figure 1. SEM images of fibers: a-d) PI fiber coated with PEDOT:PSS; e-h) PI fiber coated with PEDOT:PSS/p-type Bi_2Te_3 .

In this work, PI paper and commercial typing paper were selected to act as substrate for the 3-D printed f-TEGs. The deposition of Bi_2Te_3 (p-type)/ PEDOT:PSS TE thick films using a 3-D printing technique consists of several steps: 3-D printing, drying, and annealing. Figure 2 shows the simulated images of TE leg of 3-D printing. TE leg dimension: 30mm*4mm*0.05mm. After printing, the printed film is dried at 50 °C for 30min, 70 °C for 30min, 90 °C for 30min to remove organic residues, and then undergo an annealing process at 115 °C in a vacuum environment. The purpose of the annealing time

programming is to increase the adhesion between the substrate and the paste and reduce the porous insulation so that the paste would not be delaminated after annealing.



Figure 2 Simulated images of P-type TE leg

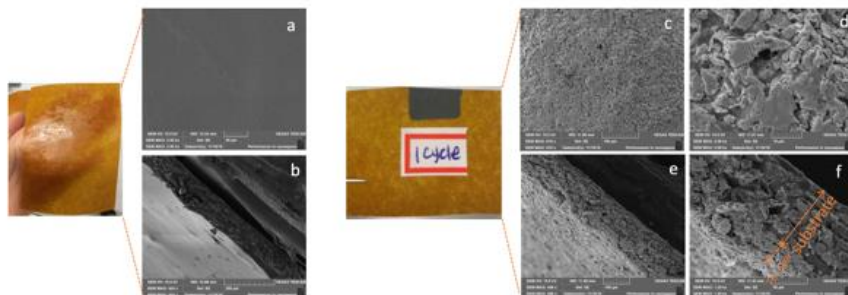


Figure 3 SEM images of SEM images of PI paper coated with PDMS: (a) positive side; (b) cross-section; PI paper coated with TE materials:(c-d) positive side; e-f) cross-section view.

For the commercial typing paper, it can be used without any further treatment. However, in terms of PI paper, since there are some fibres on PI paper, we could not use PI for printing directly. PDMS is the most widely used silicon-based organic polymer, and is particularly known for its unusual rheological (or flow) properties. It can flow to cover the surface and mould to any surface imperfections. In order to smooth the uneven PI paper, PDMS was employed to pre-treat the substrate. Figure 3a,b show positive side and cross-section of PDMS- treated paper. After PDMS treatment, superficial structure of PI paper demonstrated smooth and uniform. Flowing PDMS solution covered the surface, filling the imperfection which was caused by fibres. Figure 3c-f showed the positive side and cross-section of 3-D printed TE film. A p-type $\text{Bi}_2\text{Te}_3/\text{PEDOT:PSS}$ film coated on the PI paper was cut into thin strips for SEM observation. The pattern printed on paper had good resolution and good adhesion. The thickness of film was about $50\ \mu\text{m}$. The printed

TE film was compact and continues although there were some defects on it which will increase electric resistance.



Figure 4. Flexible TE film fabricated on (a) water-soluble paper, (b) typing paper and (c) PI paper. The dimension of these three legs is 30mm*4mm*0.05mm.

Table 1 Resistance of TE film based on different substrates

Substrate	Water-soluble paper	Typing paper	PI paper
Sheet resistance (Ω/\square)	172	374	445

The dimension of 30mm* 4mm with thickness of 50 μm of TE leg was printed on the water-soluble paper, typing paper and PI paper successfully (Figure. 4). The printed film maintained the excellent flexibility which can be easily rolled up and bent. In addition, the printed TE films demonstrated a slightly variation on the sheet resistance based on different substrates. From the table 1, the sheet resistance of water-soluble paper, typing paper, and PI paper based TE film increased lightly in sequence. Since the sheet resistance quantifies the ability for charge to go through uniform thin films, the uneven substrate would cause the TE film discontinuity which decreased the electrical conductivity of the thin films. It is shown that the pre-treatment PI paper was more roughness than water-soluble paper and typing paper, inducing some leakage connection during printing process. This pre-treatment strategy can ensure the good resolution and good adhesion in printing procedure while it still could not remove the unevenness of the paper entirely.

Output performance of a flexible TEG module

From the introduction it can be seen that the figure of merit consists three parameters: the Seebeck coefficient α , the electrical resistivity ρ , and thermal conductivity λ . In this

typical experiment, Van der pauw measurement was used to test the transport properties and electric conductivity (α) of the printed film. The seebeck voltage of the printed sample devices were tested by a home-made set-up shown in figure 5a. The Seebeck voltage of the device was measured using a digital multimeter (Keithley 2700) with the constant temperature gradient. The temperature gradient across the sample were using digital thermometer (Anbat AT4516) with dual K input. Figure 5b illustrates the standard configuration of thermoelectric devices. Heat transfer will take place on the surface of each material when there is a temperature difference. Actually, upon closer inspection, the contacting surfaces of fibrous materials are somewhat roughness or non-conforming, making the real contact area is smaller than the corresponding contact area. Thus, the surface roughness introduces air gaps between contacting materials, resulting porous insulation. The thermal conductivity of micro-gaps, such as air, is typically much lower than that of common solid materials. Therefore, the conduction of heat flux in non-conducting regions is smaller than entire contact areas, leading to increased interfacial thermal resistance. In this measurement, all mechanical interfaces were sealed with thermal compound to reduce heat loss. All tests were processed in open air at room temperature. A single thermoleg with this dimension can generate a voltage of 5.38 mV at a temperature difference of 70 K (Figure 6). The calculated Seebeck coefficient of a single thermoleg is $76.86 \mu\text{V/K}$.

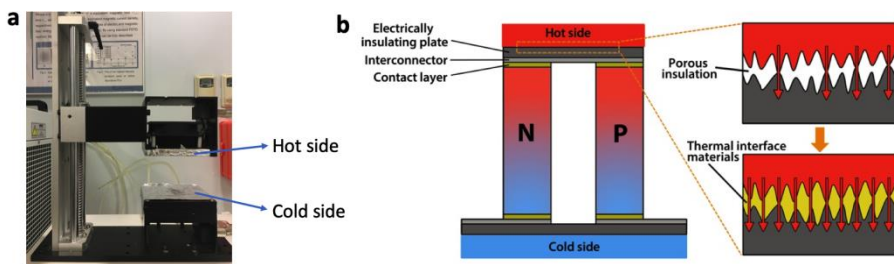


Figure 5 (a) Lab-made Seebeck Voltage measurement setup. (b) Standard configuration of thermoelectric devices.

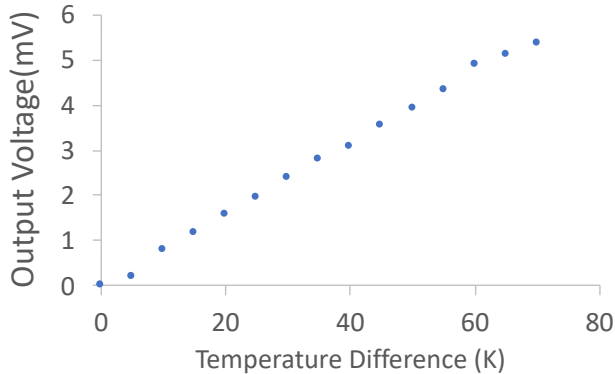


Figure 6 Output voltage of the p-type Bi₂Te₃/ PEDOT:PSS TE film.

Conclusions:

This work demonstrates that the low cost 3-D printing technology can be used to fabricate f-TEGs for room temperature energy harvesting applications. A single thermoleg with this dimension can generate a voltage of 5.38 mV at a temperature difference of 88 K. Then, higher power output can be achieved by deploying more thermolegs in layer by layer. However, the high and increasing electrical resistivity of printed thermoelectric film is an issue for reaching a higher power output for printed f-TEGs. Future work will also explore the optimization of design and material processing to decrease the resistivity.

Acknowledgements:

The authors acknowledge partial funding support from Hong Kong Research Grants Council (grant no. 15204715) and the Hong Kong Polytechnic University (grant no: bba3). SP Lin is grateful for a postgraduate scholarship from the Hong Kong Polytechnic University.

REFERENCES:

- [1] W. Zeng, X.M. Tao, S.P. Lin, C. Lee, D.L. Shi, K.H. Lam, B.L. Huang, Q.M. Wang, Y. Zhao, *Nano Energy*, 54 (2018) 163-174.
- [2] Y. Lu, Y.F. Ding, Y. Qiu, K.F. Cai, Q. Yao, H.J. Song, L. Tong, J.Q. He, L.D. Chen, *Acs Appl Mater Inter*, 11 (2019) 12819-12829.
- [3] Q.P. Wan, Y.K. Teh, Y. Gao, P.K.T. Mok, *IEEE T Circuits-I*, 64 (2017) 2346-2358.
- [4] Q.P. Wan, P.K.T. Mok, *Ieee Cust Integr Cir*, (2018).
- [5] L.S. Zhang, S.P. Lin, T. Hua, B.L. Huang, S.R. Liu, X.M. Tao, *Adv Energy Mater*, 8 (2018).
- [6] J. Choi, Y. Jung, S.J. Yang, J.Y. Oh, J. Oh, K. Jo, J.G. Son, S.E. Moon, C.R. Park, H. Kim, *Acs Nano*, 11 (2017) 7608-7614.
- [7] Y.F. Ding, Y. Qiu, K.F. Cai, Q. Yao, S. Chen, L.D. Chen, J.Q. He, *Nat Commun*, 10 (2019).
- [8] J.F. Li, W.S. Liu, L.D. Zhao, M. Zhou, *Npg Asia Mater*, 2 (2010) 152-158.
- [9] M. He, F. Qiu, Z.Q. Lin, *Energ Environ Sci*, 6 (2013) 1352-1361.
- [10] S.J. Kim, J.H. We, B.J. Cho, *Energ Environ Sci*, 7 (2014) 1959-1965.
- [11] Z.U. Khan, O. Bubnova, M.J. Jafari, R. Brooke, X.J. Liu, R. Gabrielsson, T. Ederth, D.R. Evans, J.W. Andreasen, M. Fahlman, X. Crispin, *J Mater Chem C*, 3 (2015) 10616-10623.
- [12] D. Zhao, A. Martinelli, A. Willfahrt, T. Fischer, D. Bernin, Z.U. Khan, M. Shahi, J. Brill, M.P. Jonsson, S. Fabiano, X. Crispin, *Nat Commun*, 10 (2019).
- [13] R. Venkatasubramanian, E. Siivola, T. Colpitts, B. O'Quinn, *Nature*, 413 (2001) 597-602.
- [14] R.G. Deng, X.L. Su, S.Q. Hao, Z. Zheng, M. Zhang, H.Y. Xie, W. Liu, Y.G. Yan, C. Wolverton, C. Uher, M.G. Kanatzidis, X.F. Tang, *Energ Environ Sci*, 11 (2018) 1520-1535.
- [15] T. Park, C. Park, B. Kim, H. Shin, E. Kim, *Energ Environ Sci*, 6 (2013) 788-792.
- [16] A.M. Nardes, M. Kemerink, R.A.J. Janssen, J.A.M. Bastiaansen, N.M.M. Kiggen, B.M.W. Langeveld, A.J.J.M. van Breemen, M.M. de Kok, *Adv Mater*, 19 (2007) 1196-+.
- [17] S.L. Kim, K. Choi, A. Tazebay, C. Yu, *Acs Nano*, 8 (2014) 2377-2386.
- [18] K. Ahmad, C. Wan, M.A. Al-Eshaikh, A.N. Kadachi, *Appl Surf Sci*, 474 (2019) 2-8.
- [19] T. Juntunen, H. Jussila, M. Ruoho, S.H. Liu, G.H. Hu, T. Albrow-Owen, L.W.T. Ng, R.C.T. Howe, T. Hasan, Z.P. Sun, I. Tittonen, *Adv Funct Mater*, 28 (2018).
- [20] M.X. Piao, G. Kim, G.P. Kennedy, S. Roth, U. Dettlaff-Weglikowska, *Phys Status Solidi B*, 250 (2013) 2529-2534.